J Biomol NMR (2007) 38:199–212
DOI 10.1007/s10858-007-9158-6

ARTICLE

Fractional ^{13}C enrichment of isolated carbons using [1-^{13}C]- or [2-^{13}C]-glucose facilitates the accurate measurement of dynamics at backbone C^{α} and side-chain methyl positions in proteins

Patrik Lundström · Kaare Teilum · Tommy Carstensen · Irina Bezsonova · Silke Wiesner · D. Flemming Hansen · Tomasz L. Religa · Mikael Akke · Lewis E. Kay

Revised: 30 March 2007 / Accepted: 2 April 2007 / Published online: 7 June 2007

Abstract A simple labeling approach is presented based on protein expression in [1-^{13}C]- or [2-^{13}C]-glucose containing media that produces molecules enriched at methyl carbon positions or backbone C^{α} sites, respectively. All of the methyl groups, with the exception of Thr and Ile(δ1) are produced with isolated ^{13}C spins (i.e., no ^{13}C–^{13}C one bond couplings), facilitating studies of dynamics through the use of spin-spin relaxation experiments without artifacts introduced by evolution due to large homonuclear scalar couplings. Carbon-α sites are labeled without concomitant labeling at C^{β} positions for 17 of the common 20 amino acids and there are no cases for which $^{13}C^{\alpha}$–^{13}CO spin pairs are observed. A large number of probes are thus available for the study of protein dynamics with the results obtained complimenting those from more traditional backbone ^{15}N studies. The utility of the labeling is established by recording ^{13}C $R_{1\rho}$ and CPMG-based experiments on a number of different protein systems.

Keywords Selective ^{13}C labeling · Protein expression · [1-^{13}C]-glucose · [2-^{13}C]-glucose · ^{13}C relaxation measurements · CPMG relaxation dispersion · $T_{1\rho}$

P. Lundström · D. F. Hansen · L. E. Kay (✉)
Departments of Medical Genetics and Chemistry,
The University of Toronto, Toronto, ON, Canada M5S 1A8
e-mail: kay@pound.med.utoronto.ca

P. Lundström · S. Wiesner · D. F. Hansen · L. E. Kay
Department of Biochemistry, The University of Toronto,
Toronto, ON, Canada M5S 1A8

K. Teilum · T. Carstensen · M. Akke
Department of Biophysical Chemistry, Lund University,
Lund SE-22100, Sweden

I. Bezsonova
Department of Chemistry, The University of Toronto,
Toronto, ON, Canada M5S 1A8

I. Bezsonova · S. Wiesner
Program in Molecular Structure and Function, The Hospital for Sick Children, Toronto, ON, Canada M5G 1X8

T. L. Religa
Medical Research Council Centre for Protein Engineering,
Hills Road, Cambridge CB2 2QH, UK

Introduction

NMR spectroscopy is a particularly powerful tool for probing protein dynamics over a wide range of biologically relevant time-scales (Mittermaier and Kay 2006; Palmer 2004; Peng and Wagner 1994; Torchia and Ishima 2003). The most common approach involves the interpretation of spin relaxation rates in terms of dynamics parameters that report on the time-scale(s) and amplitude(s) of ps-ns motions (Kay et al. 1989). However other classes of relaxation experiments that are sensitive to μs-ms time-scale dynamics have been developed that provide insight into the kinetics and thermodynamics of exchange processes along with information relating to the structures of the interconverting sites (Palmer et al. 2001). NMR studies that probe motional processes in biological molecules have benefited tremendously from the incorporation of label, either uniformly or specifically, leading to spectra of high sensitivity from which quantitative inferences can be made.

To date most studies of protein dynamics have focused on backbone amide nitrogens in uniformly ^{15}N labeled molecules. The high sensitivity of two-dimensional ^{1}H–^{15}N correlation spectra, the ease of ^{15}N incorporation and the fact that the relaxation of the amide nitrogen is dominated

by contributions that derive from interactions exclusive to the ^{1}H–^{15}N one bond coupled spin pair have all contributed to the popularity of this approach. Yet it is increasingly clear that the picture of protein dynamics that emerges from ^{15}N spin relaxation studies is incomplete. For example, the ^{1}H–^{15}N amide vector may be insensitive to large classes of motions that involve side-chains, for example, or even motions of the backbone that specifically lead to reorientation along an axis that is parallel to the amide vector direction (Wang et al. 2003). In the case of relaxation dispersion experiments that measure changes in chemical shifts between exchanging sites, the interpretation of such shift changes from ^{15}N experiments is complicated by the fact that they depend on secondary structure *and* on additional factors such as hydrogen bonding and χ_1 dihedral angles (Le and Oldfield 1994; Xu and Case 2002). In contrast, the chemical shifts of $^{13}C^{\alpha}$ spins depend on backbone dihedral angles in a well known way (Spera and Bax 1991; Wishart and Sykes 1994) so that direct structural information is available from ^{13}C NMR.

Despite the fact that there are many more carbon than nitrogen probes in a protein, ^{13}C relaxation experiments have not enjoyed the popularity of their ^{15}N counterparts, in large measure because of difficulties in achieving a suitable labeling pattern that can be exploited in a straightforward manner experimentally. For example, uniformly ^{13}C labeled samples can be easily produced, but the large one bond ^{13}C–^{13}C couplings impose significant constraints on experimental design. We have shown previously that $^{13}C^{\alpha}$ R_1, $R_{1\rho}$ and $^{1}H^{\alpha}$–$^{13}C^{\alpha}$ steady state NOE measurements can be made on uniformly ^{13}C labeled protein samples with suitable precautions, although their interpretation is more complicated than is the case for backbone ^{15}N spins (Yamazaki et al. 1994); subsequently other applications involving relaxation measurements on uniformly ^{13}C labeled protein samples have emerged (Brath et al. 2006; Cordier et al. 1996; Fruh et al. 2001; Zeng et al. 1996). However, the preparation of samples lacking ^{13}C–^{13}C one-bond coupled spin pairs remains a prerequisite for certain applications such as ^{13}C CPMG-based relaxation dispersion experiments for the quantification of millisecond (ms) time-scale processes. Selective labeling is also very beneficial for off-resonance $R_{1\rho}$ dispersion studies that measure μs dynamics.

Selectively ^{13}C labeled proteins must, of course, be prepared by using growth media based on carbon sources other than uniformly ^{13}C labeled glucose. Such media can be comprised of mixtures of labeled and unlabeled acetates (Wand et al. 1995), either [2-^{13}C]- or [1,3-$^{13}C_2$]-glycerol (LeMaster and Kushlan 1996), or selectively labeled precursors such as [3-^{13}C]-pyruvate (Ishima et al. 2001; Lee et al. 1997; Mulder et al. 2002) or [1-^{13}C]-glucose (Glc) (Teilum et al. 2006). Of the different media that are available for growth Glc is among the most common and often produces high yields of protein expression. With this in mind we focus here on the production of ^{13}C labeled proteins using selectively labeled Glc as the carbon source. In particular, our present interest is on samples with ^{13}C enrichment at either α- or methyl carbons since previous experience has shown that these positions are particularly valuable probes of protein dynamics (Mulder et al. 2001; Nicholson et al. 1992; Yamazaki et al. 1994). In this regard, we show that protein expression in media where [2-^{13}C]-Glc is the exclusive carbon source leads to 20–45% ^{13}C enrichment at the C^{α} position without labeling of CO sites for all residues or labeling of C^{β} for all residues except Leu, Val and Ile; Leu can be selectively enriched at C^{α} using [1-^{13}C]-Glc. It is also shown that [1-^{13}C]-Glc leads to ~45% selective enrichment of the methyl carbons of Ala, Val, Leu, Met and Ile ($C^{\gamma 2}$ only) that are in turn separated by two or more covalent bonds from other ^{13}C enriched positions. The relevant metabolic pathways that give rise to labeling are discussed in relation to the expected labeling patterns. These labeling patterns are subsequently verified by experiment and a number of applications are briefly described.

Material and methods

Sample preparation

A number of protein samples were produced using either [1-^{13}C]-Glc, [2-^{13}C]-Glc or U-^{13}C-Glc as the carbon source, with uniform ^{15}N labeling. These include the F61A/A90G mutant of Rd-apocytochrome b_{562} (Chu et al. 2002), human ubiquitin (Di Stefano and Wand 1987), the FF domain from the human protein FBP11 (Jemth et al. 2005) and the bovine acyl Co-A binding protein, ACBP (Mandrup et al. 1991). All proteins were expressed in BL21(DE3) cells, with the exception of the FF domain that was produced in JM109(DE3) cells and purified according to standard protocols that have been described previously and discussed in the references listed above. Sample conditions were as follows: F61A/A90G mutant of Rd-apocytochrome b_{562}: 1.4 mM protein in 50 mM Na-acetate, pH 4.8, 5% D_2O; ubiquitin: 0.8 mM protein, 10 mM P_i, pH 6.6, 10% D_2O; FF domain: 1.0 mM protein, 50 mM Na-acetate, 100 mM NaCl, 0.05% NaN_3, 0.2 mM EDTA, pH 5.7, 10% D_2O; ACBP: 1 mM (protonated sample) or 0.6 mM (partly deuterated sample) protein in 20 mM Na-acetate, pH 5.3, 10% D_2O.

NMR spectroscopy

The fractional ^{13}C enrichment at C^{α} and methyl positions was determined by comparing the intensities of resonances

in ^{13}C-HSQC spectra of samples produced using either [2-^{13}C]-Glc (ubiquitin and the FF domain) or [1-^{13}C]-Glc (ACBP and FF domain), respectively, with intensities of correlations from spectra of protein samples generated using uniformly ^{13}C labeled glucose. To account for different sample concentrations, the intensities were first normalized by the average signal intensity in ^{15}N-HSQC data sets (all proteins were U-^{15}N labeled). The fractional enrichment at position i is defined as $E_i = (C_{s,i}/N_s)/(C_{u,i}/N_u)$, where $C_{s,i}$ and $C_{u,i}$ are the peak intensities of resonance i in ^{13}C-HSQC data sets of the selectively and uniformly labeled samples respectively, that were recorded identically, N_s and N_u are normalization factors corresponding to the average of peak intensities in ^{15}N-HSQC data sets of the different samples. Note that in the small number of cases where both singlet and doublet multiplet components are observed (Ile and Val residues for $^{13}C^{\alpha}$ labeling and Thr, Ile(δ1) for methyl labeling) $C_{s,i}$ is the sum of over all multiplet components (i.e., singlets and doublets; see below).

A ^{13}C-HSQC data set was recorded to obtain a qualitative estimate of the isotopomer composition of the methyl groups of the ACBP sample produced in D_2O. Corrections for differential relaxation of the isotopomers were not made.

CPMG relaxation dispersion profiles for all proteins were recorded at a pair of magnetic field strengths corresponding to ^{1}H resonance frequencies of 500 and 800 MHz with the exception of data sets for ACBP where fields corresponding to 500 and 600 MHz were employed. All spectrometers were equipped with room temperature probe heads. $^{13}C^{\alpha}$ CPMG data sets for the F61A/A90G mutant of Rd-apocytochrome b_{562} produced with [2-^{13}C]-Glc as the carbon source were recorded at 45°C using a relaxation-compensated pulse sequence (Loria et al. 1999) with REBURP (Geen and Freeman 1991) refocusing pulses of duration 460 μs (500 MHz) and 350 μs (800 MHz). A constant-time relaxation delay of 16 ms was employed along with ν_{CPMG} values between 125 Hz and 1 kHz. Typically 8 dispersion points were recorded, along with 3 repeat values for error analysis, with an acquisition time of 3.5 h for each 2D data set (ν_{CPMG} value). Methyl CPMG dispersion profiles for the FF domain produced with [1-^{13}C]-Glc were recorded at 30°C using a variant of the scheme of Skrynnikov et al. (2001) where magnetization originates on ^{1}H (Lundström et al. 2007), with a constant-time relaxation delay of 30 ms, ν_{CPMG} values that varied between 66 Hz and 1 kHz and with REBURP refocusing pulses of the same duration as those used in the C^{α} experiments. A total of 12 ν_{CPMG} values were recorded, with each 2D data set acquired in 0.4 h. ^{13}C methyl relaxation dispersion profiles (Skrynnikov et al. 2001) were obtained for ACBP (fully protonated sample) at 40 °C with a constant-time relaxation delay of 40 ms and 16 ν_{CPMG} values between 50 Hz and 900 Hz (1.9 h/2D data set). $R_{1\rho}$ experiments (Brath et al. 2006) for the ACBP sample produced in D_2O were recorded at 500 MHz, employing multiple spin-lock fields (386, 759, 947, 1237, 1729, 2824 Hz) and carrier offsets (0, ±500, ±1000, –1500, –2000, –4000, –10000, –20000 Hz), as described previously (Brath et al. 2006). Each of the 2D data sets used to define the dispersion profiles was recorded in 0.7 h.

$^{13}C^{\alpha}$ R_1 and $R_{1\rho}$ relaxation rates were measured for ubiquitin at 25°C, 800 MHz using standard pulse sequences that were adapted from ^{15}N to ^{13}C. Relaxation delays for the R_1 experiments varied between 10 ms and 500 ms, while those for the $R_{1\rho}$ experiment (spin-lock field of $\gamma B_1/2\pi$ = 1790 Hz with the carrier positioned at 58.2 ppm) varied from 1 to 50 ms. Each of the R_1 and $R_{1\rho}$ experiments was acquired in 2.6 and 3.5 h, respectively.

All data were processed and analyzed with the nmrPipe/nmrDraw suite of programs (Delaglio et al. 1995) and SPARKY (Goddard and Kneller), as described previously (Korzhnev et al. 2004; Mulder et al. 2002). R_1 and $R_{1\rho}$ decays were fitted to a mono-exponential function, while dispersion profiles were fitted to a model that assumes a global two state exchange process using in-house software that is available upon request. Errors in peak intensities were estimated from multiple measurements, as described above, and propagated to errors in the effective relaxation rate, $R_{2,eff}(\nu_{CPMG})$ (Korzhnev et al. 2004). A minimum error of 2% was imposed on $R_{2,eff}(\nu_{CPMG})$. Errors in the model parameters were estimated using the covariance matrix approach (Press et al. 1988).

Results and discussion

In this study we describe the use of [1-^{13}C]- or [2-^{13}C]-Glc media for the expression of proteins that are fractionally enriched with ^{13}C at a large number of positions, and with only a few exceptions, with label that is separated by at least two covalent bonds. Our primary interest is to generate proteins with ^{13}C label at C^{α} and methyl positions that can then be used in a variety of spin-relaxation experiments.

The metabolic pathways for amino acid biosynthesis in *E. coli* are well known and comprehensively described in biochemistry textbooks (Voet and Voet 1995). For completeness, in Fig. 1a we start from [2-^{13}C]-Glc and highlight some of the steps in glycolysis and in the tricarboxylic acid cycle (TCA cycle) that produce ^{13}C enrichment at the C^{α} positions in amino acids. Briefly, the amino acids can be grouped into three categories based on their metabolic precursors. Ala, Cys, Gly, Lys, Ser, Val as well as the aliphatic moieties of Phe, Trp and Tyr originate from the

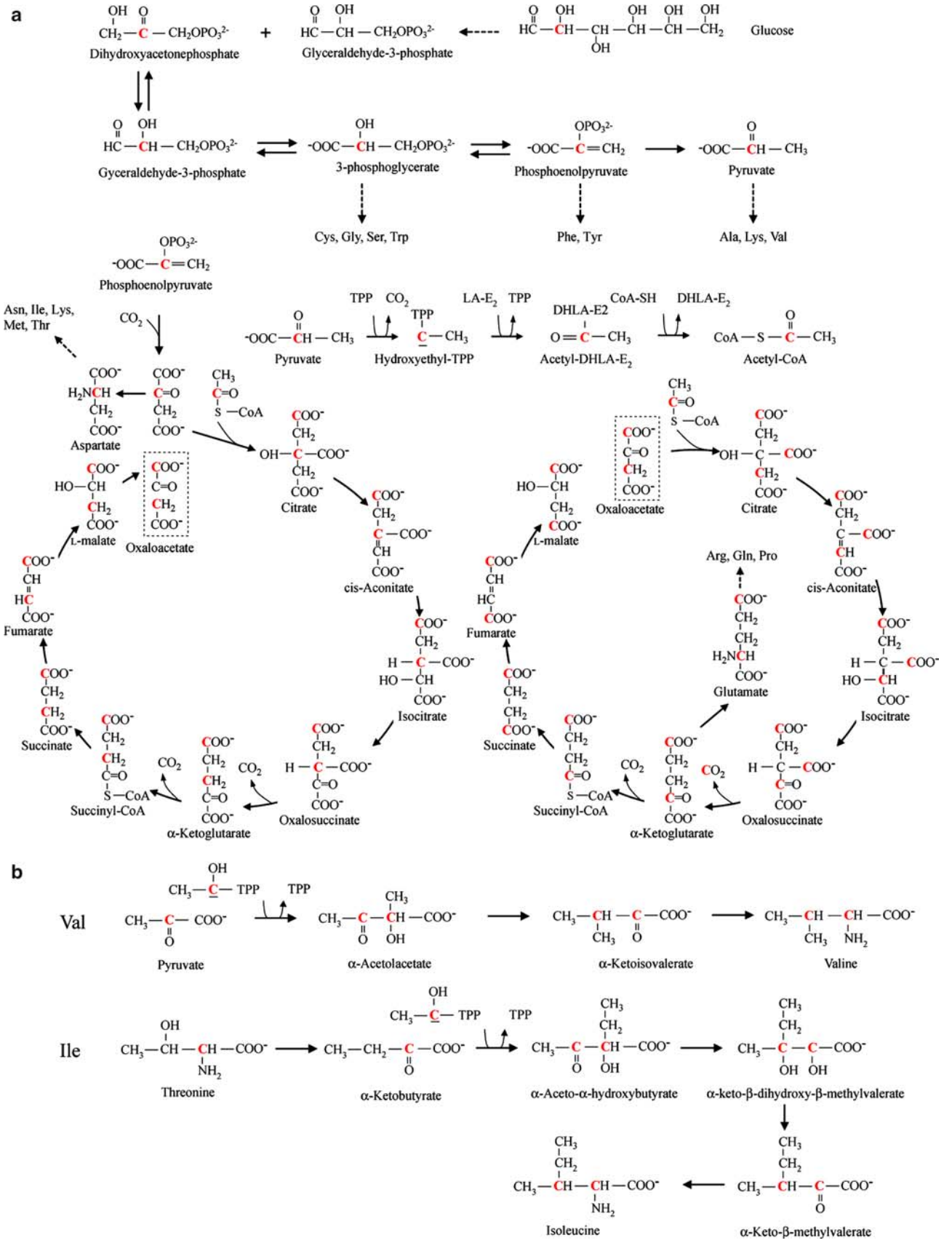
a
Dihydroxyacetonephosphate
Glyceraldehyde-3-phosphate
Glucose
Gyceraldehyde-3-phosphate
3-phosphoglycerate
Phosphoenolpyruvate
Pyruvate
Cys, Gly, Ser, Trp
Phe, Tyr
Ala, Lys, Val
Asn, Ile, Lys, Met, Thr
TPP
LA-E2
CoA-SH
DHLA-E2
Hydroxyethyl-TPP
Acetyl-DHLA-E2
Acetyl-CoA
Aspartate
L-malate
Oxaloacetate
Citrate
cis-Aconitate
Isocitrate
Fumarate
Succinate
Succinyl-CoA
α-Ketoglutarate
Oxalosuccinate
Arg, Gln, Pro
Glutamate
b
Val
Pyruvate
α-Acetolactate
α-Ketoisovalerate
Valine
Ile
Threonine
α-Ketobutyrate
α-Aceto-α-hydroxybutyrate
α-keto-β-dihydroxy-β-methylvalerate
α-Keto-β-methylvalerate
Isoleucine

◀**Fig. 1** Major biosynthetic pathways involved in C^{α} labeling of amino acids, showing key steps in glycolysis (top 2 rows) and the TCA cycle. Intermediates in glycolysis and the TCA cycle are precursors for the backbone of 19 of the amino acid (His is the only exception). [2-^{13}C]-Glc results in ^{13}C enrichment at C^{α} positions of all these residues except Leu and simultaneous enrichment at C^{α} and C^{β} only occurs for Ile and Val. Carbons that are highlighted in red are those that are ^{13}C enriched. (**a**) Glycolysis and the TCA cycle. Glucose is metabolized to pyruvate that is decarboxylated via the intermediates hydroxyethyl-TPP (thiamine pyrophosphate) and acetyl-DHLA-E2 (dihydrolipoamide) to yield acetyl-S-CoA. The acetyl group of acetyl-S-CoA then fuses with oxaloacetate, which is produced by carboxylation of the glycolysis intermediate phosphoenolpyruvate, to form citrate that enters the TCA cycle. The net result of the TCA cycle is two decarboxylations and regeneration of oxaloacetate. The oxaloacetate product of the first round of the TCA cycle (shown to the left) fuses with another acetyl group and enters the next round (shown to the right). (**b**) For Ile and Val, C^{α} and C^{β} originate from two different molecules and may be independently ^{13}C enriched. Thus, in a fraction of these amino acids both C^{α} and C^{β}positions will be ^{13}C labeled

glycolytic three-carbon metabolites pyruvate (Ala, Lys, Val), 3-phosphoglycerate (3PG; Cys, Gly, Ser, Trp) and phosphoenolpyruvate (PEP; Phe and Tyr). The labeling patterns and incorporation levels for these amino acids are readily predicted, because there is minimal scrambling of the carbon atoms from Glc to the three-carbon glycolytic precursors. The rapid equilibrium between dihydroxyacetonephosphate (DHAP) and glyceraldehyde-3-phosphate (GAP) due to their isomerization (top 2 lines of Fig. 1), leads to approximately 50% enrichment at C^{α} for the above-mentioned residues.

The labeling patterns for the remaining residues are somewhat more difficult to predict since they are derived from intermediates of the TCA cycle. For example, consider the fate of oxaloacetate (OA) that is the precursor of Asn, Asp, Ile, Lys, Met and Thr, Fig. 1a. Following the steps of Fig. 1a OA produced from 2-^{13}C PEP will be labeled exclusively at the 2-position and a number of possibilities for this molecule subsequently arise, including transamination without entry into the TCA cycle, transamination after one TCA cycle (left hand TCA in Fig. 1a) or transamination after a pair of TCA cycles (left hand TCA, followed by right hand TCA):

$$2\text{-}^{13}\mathrm{C\,OA} \xrightarrow{\text{Transamination}} 2\text{-}^{13}\mathrm{C\,Asp}$$

$$2\text{-}^{13}\mathrm{C\,OA} \xrightarrow{\text{1 round of TCA}} 1,3\text{-}^{13}\mathrm{C\,OA}$$

$$\text{or } 2,4\text{-}^{13}\mathrm{C\,OA} \xrightarrow{\text{Transamination}} 1,3\text{-}^{13}\mathrm{C\,Asp} \text{ or } 2,4\text{-}^{13}\mathrm{C\,Asp}$$

$$2\text{-}^{13}\mathrm{C\,OA} \xrightarrow{\text{2 rounds of TCA}} 1,4\text{-}^{13}\mathrm{C\,OA} \text{ or } 1,3\text{-}^{13}\mathrm{C\,OA}$$

$$\text{or } 2,4\text{-}^{13}\mathrm{C\,OA} \xrightarrow{\text{Transamination}} 1,4\text{-}^{13}\mathrm{C\,Asp}$$

$$\text{or } 1,3\text{-}^{13}\mathrm{C\,Asp} \text{ or } 2,4\text{-}^{13}\mathrm{C\,Asp}$$

Note that the TCA metabolite succinate is symmetric so that the 1,3-^{13}C labeling shown for this molecule in Fig. 1a, left TCA cycle, is equivalent to 2,4-^{13}C labeling so that either 1,3- or 2,4-^{13}C Asp is produced after a single round of the TCA cycle. Thus, both $^{13}C^{\alpha}$ and $^{13}C^{\gamma}$ (or ^{13}CO and $^{13}C^{\beta}$) can be labeled in the same residue, although on average labeling at the C^{α} position is higher than at C^{γ}, but less than 50%. A similar analysis of the fate of α-ketoglutarate (AKG) that is the precursor for Arg, Gln, Glu and Pro shows that residues from this precursor that are labeled at the C^{α} position can also be labeled at the C^{δ} position after two rounds of the TCA cycle (right hand cycle in Fig. 1a); no labeling at C^{α} is produced after a single TCA cycle. For all residues excluding Ile and Val, $^{13}C^{\alpha}$–$^{13}C^{\beta}$ couplings are not predicted nor observed in experiments (see below). Figure 1b illustrates the relevant metabolic pathways for Ile and Val showing how label at both C^{α} and C^{β} can be incorporated into these residues. It is worth noting that each of the two initial precursors of Val in the scheme of Fig. 1b has a 50% chance of containing ^{13}C label since they ultimately derive from DHAP, Fig. 1a, that has a 50% probability of being labeled. Thus it is expected that Val produced in this manner would be $^{13}C^{\alpha}$–$^{13}C^{\beta}$ (25%, illustrated in Fig. 1b), $^{13}C^{\alpha}$–$^{12}C^{\beta}$ (25%), $^{12}C^{\alpha}$–$^{13}C^{\beta}$ (25%) and $^{12}C^{\alpha}$–$^{12}C^{\beta}$ (25%). Ile can also be labeled at $^{13}C^{\alpha}$ and $^{13}C^{\beta}$ positions simultaneously with a predicted probability of somewhat less than 25% (Fig. 1b). Of interest, Leu residues are predicted not to be labeled at the C^{α} position using the [2-^{13}C]-Glc precursor, although $^{13}C^{\alpha}$-Leu can be synthesized from [1-^{13}C]-Glc, as shown below. It is worth noting that residues labeled with ^{13}C at the C^{α} position will not be ^{13}C labeled at the carbonyl carbon.

In a previous publication we have shown that protein expression with [1-^{13}C]-Glc leads to aromatic labeling patterns that are devoid of ^{13}C–^{13}C one-bond couplings, facilitating the measurement of aromatic ^{13}C off-resonance $R_{1\rho}$ dispersion profiles (Teilum et al. 2006). Here the main interest is that [1-^{13}C]-Glc also results in protein samples where many of the methyl carbons are labeled but where the adjacent carbons are not. Figure 2 illustrates the relevant pathways for the incorporation of ^{13}C into methyl positions of the methyl containing amino acids using [1-^{13}C]-Glc as the sole carbon source. For Ala, Leu and Val the methyl carbons are derived from pyruvate or a derivative of pyruvate (hydroxyethyl-TPP) that has a 50% chance of ^{13}C label at the methyl position so that each methyl site in these amino acids is predicted to be labeled to 50%. In the case of Leu an isolated ^{13}C label at the C^{α} position can be obtained in addition to methyl labeling that can be used to probe backbone dynamics. The methyl carbon of Met originates from the C^{β} site of Ser that is 50% ^{13}C labeled (since it derives from 3 phosphoglycerate that is 50% ^{13}C labeled at the 3 position when *E. coli* are grown

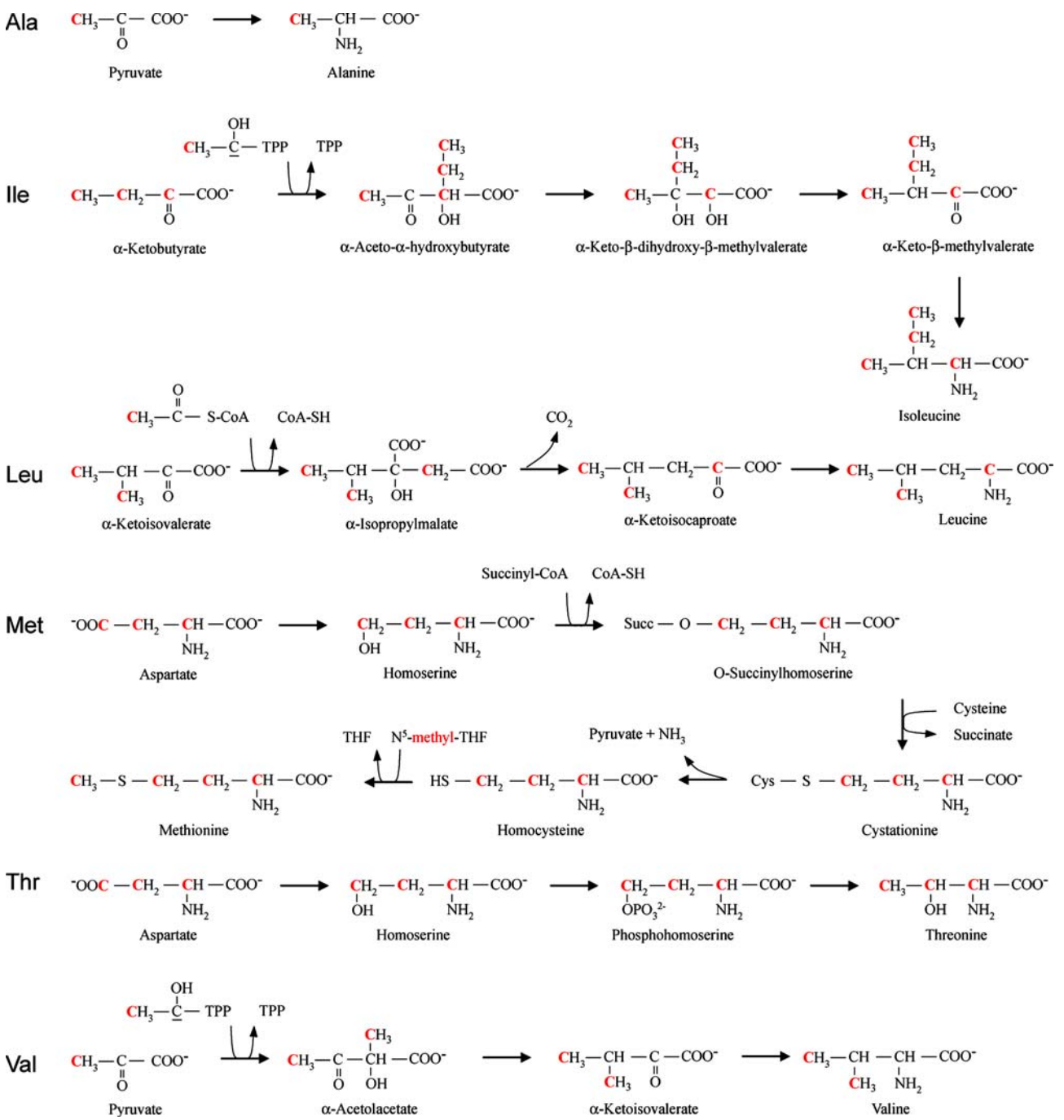

Fig. 2 Biosynthesis of amino acids with methyl side-chains. Carbons in red indicate ^{13}C enriched positions when [1-^{13}C]-Glc is used as the carbon source. The labeling pattern of Asp, which is the precursor of Ile, Met and Thr, depends on how oxaloacetate (OA) from which it derives was synthesized (i.e., through how many rounds of the TCA cycle OA was processed). Enrichment of Ile, Met and Thr may thus be variable; shown here is the pattern that results from three rounds of the TCA cycle using a ^{13}C enriched molecule of acetyl-S-CoA in each round. The source of the methyl group of N^5-methyl-THF (tetrahydrofolate) is Ser C^{β}. The α-ketoisovalerate precursor of Leu originates from pyruvate (see Val)

on [1-^{13}C]-Glc) and consequently it is also predicted to be labeled to 50%. In contrast to the methyl containing residues discussed above Thr is derived from the TCA product OA that can be ^{13}C labeled at 3 contiguous positions using [1-^{13}C]-Glc as the carbon source, Fig. 2. In general the labeling pattern for OA depends on the number of passes through the TCA cycle; after 3 passes OA (and hence Asp that derives directly from OA) can be triply ^{13}C-labeled. Since the production of Thr proceeds through the steps OA → Asp → Thr , ^{13}C–^{13}C spin pairs involving the Thr

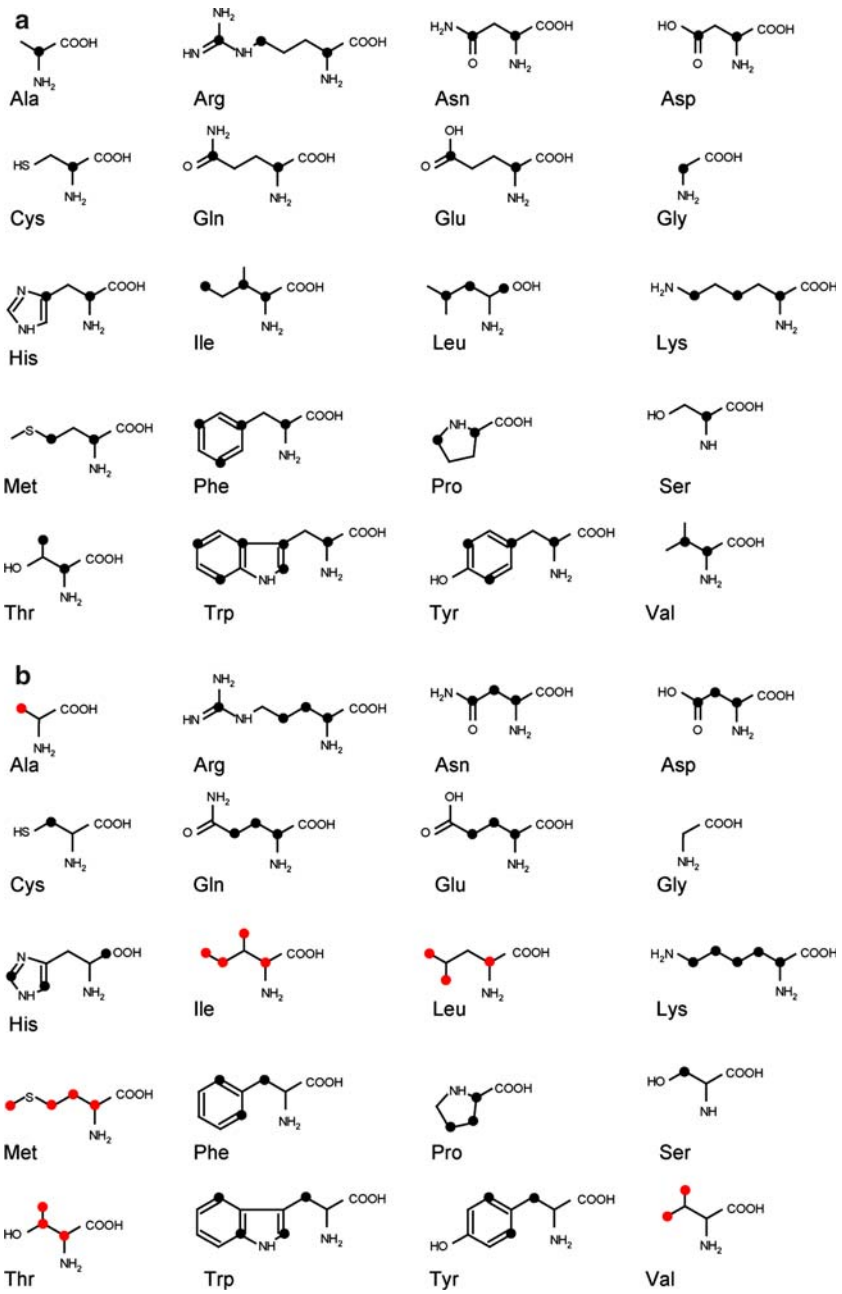

Fig. 3 Expected labeling patterns for amino acids using [2-^{13}C]-Glc (**a**) and [1-^{13}C]-Glc (**b**) as carbon sources. Circles indicate ^{13}C enriched positions. (**a**) Labeling patterns for all amino acids when [2-^{13}C]-Glc is used as the carbon source. The amino acids that are derived from TCA cycle intermediates may in principle be enriched at any position. For clarity we only show possible enriched positions that are compatible with simultaneous enrichment at C^{α} and illustrate the most complex of several labeling scenarios. (**b**) Labeling patterns for all residues when [1-^{13}C]-Glc is used as the carbon source. Enriched positions for residues with methyl side chains are highlighted in red. The most complex of several labeling scenarios is shown

methyl carbon can be generated that could potentially interfere with methyl relaxation experiments (see below). Similarly, ^{13}C label at the Ile δ1 methyl position may not be isolated, as indicated in the figure (note that the α-ketobutyrate precursor of Ile is derived from Thr). Labeling patterns for Ile, Thr that are distinct from those diagramed in Fig. 2 can be obtained, including the case where label is restricted to the methyl positions of these residues; in general, however, proteins will be produced with labeling patterns that include those that are undesired.

Figure 3a summarizes one of the labeling patterns that would be expected for proteins expressed using [2-^{13}C]-Glc in the case of interest where the C^{α} is labeled. Here we have indicated a labeling scheme that derives after at least 1 pass of precursors through the TCA cycle for OA-based residues or at least 2 passes for AKG-based amino acids using a ^{13}C enriched molecule of acetyl-S-CoA in each round; as indicated above alternative labeling occurs for OA and AKG derived residues with different numbers of passes. Figure 3b show a labeling pattern obtained after 3 passes through the TCA cycle starting from [1-^{13}C]-Glc. In general large numbers of passes through the TCA cycle maximize scrambling of label thereby increasing the likelihood of one bond ^{13}C–^{13}C couplings in amino-acids. However, the diagram of Fig. 3 is general in the sense that those $^{13}C^{\alpha}$ and ^{13}C-methyl positions that are indicated as

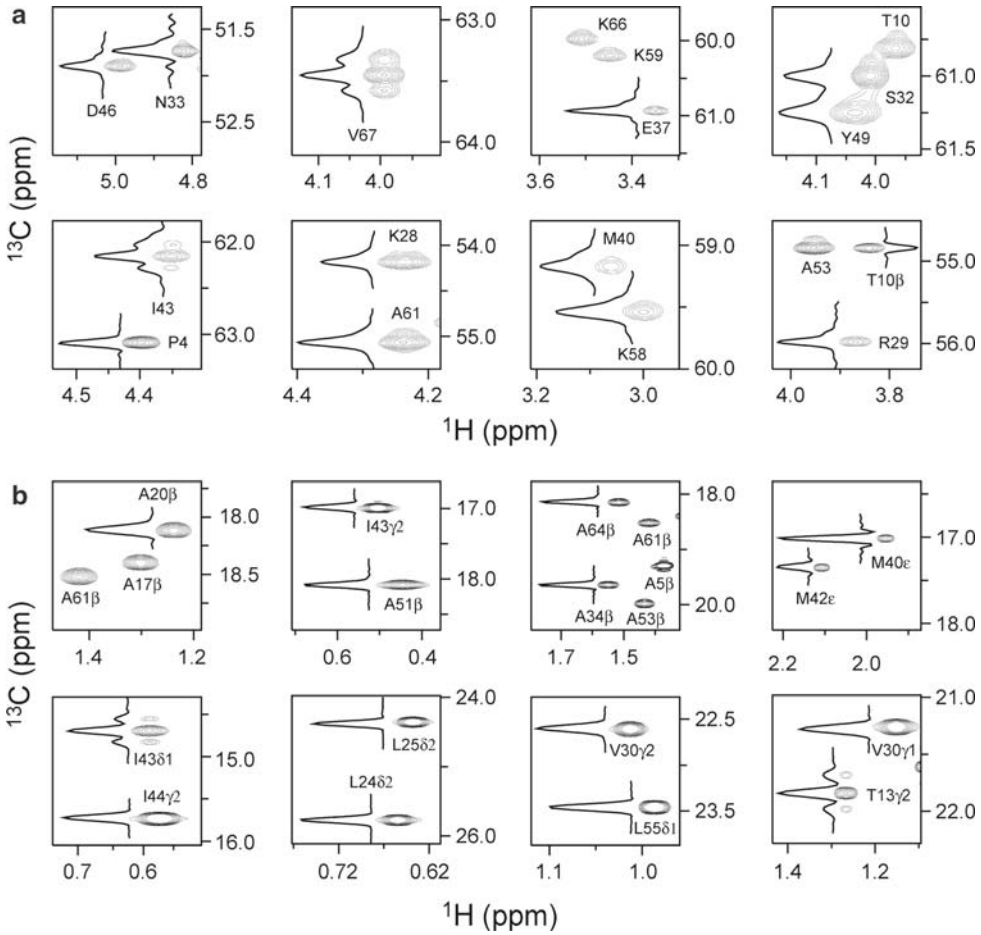

Fig. 4 Expanded correlation maps of selected C^{α} (**a**) and methyl (**b**) regions from spectra of the FBP11 FF domain; protein is grown using [2-^{13}C]-Glc (**a**) and [1-^{13}C]-Glc (**b**) as carbon sources. A singlet indicates an isolated ^{13}C enriched position whereas a doublet separated by ~35 Hz corresponds to a ^{13}C-^{13}C spin pair. More complex multiplet structures than the superposition of a singlet and a doublet were not observed. (**a**) Selected C^{α} cross-peaks and corresponding 1D traces are shown. The upfield shoulder that is noticeable for some of the resonances is due to a two bond isotope shift originating from N-D groups due to the presence of ~10% D_2O in the sample solution (Ottiger and Bax 1997). Note that this shoulder is absent for P4 and T10β (folded) (**b**) Selected methyl correlations, with examples from all 7 methyl groups shown

isolated will always be so (in a manner independent of the number of TCA cycle passes). It is clear that many sites become available for detailed relaxation studies that probe dynamics over a broad spectrum of time-scales.

We have recorded ^{1}H–^{13}C correlation spectra of a number of proteins produced using either [2-^{13}C]-Glc or [1-^{13}C]-Glc to confirm the expected labeling profiles. Figure 4a shows small expanded regions of the $^{1}H^{\alpha}$–$^{13}C^{\alpha}$ correlation map obtained for the FBP11 FF domain that has been produced using [2-^{13}C]-Glc, that illustrate the multiplet structures of individual correlations. As expected the majority of residues give rise to singlets, while Ile and Val show clearly a more complex multiplet structure that arises from a superposition of singlets ($^{13}C^{\alpha}$–$^{12}C^{\beta}$) and doublets ($^{13}C^{\alpha}$–$^{13}C^{\beta}$), as predicted would be the case from the above discussion. There are no multiplet patterns that would arise from one-bond $^{13}C^{\alpha}$–^{13}CO couplings, establishing that labeling at C^{α} and CO positions is mutually exclusive. Notably, all residue types are present in the spectrum, with the exception of Leu that is not labeled at C^{α} using [2-^{13}C]-Glc. Thus, this scheme produces isolated $^{13}C^{\alpha}$ spin labels at 17 of the 20 residues that can be used to probe molecular dynamics (see below).

The extent of incorporation of isotope label at the C^{α} positions in proteins produced using [2-^{13}C]-Glc has been quantified by measuring relative peak intensities in 'high resolution' ^{1}H–^{13}C HSQC spectra, Table 1, using a procedure that is discussed in materials and methods. In the analysis we have divided residues into the following groups based on the precursors of their backbones: Ala, Cys, Gly, Ser, Phe, Trp, Tyr Val (pyruvate, 3PG or PEP); Asn, Asp, Ile, Met, Thr (OA), Arg, Gln, Glu, Pro (AKG); His (ribose-5-phosphate); Lys (OA or pyruvate (Voet and Voet 1995)). The results in Table 1 are based on averages over all residues generated from a common set of precursors and two protein samples (ubiquitin and the FBP11 FF domain for [2-^{13}C]-Glc). Residues derived from the 3 carbon precursors (pyruvate, 3PG or PEP) are enriched at 45%, close to the value of 50% that would be predicted assuming no scrambling. In contrast, OA derived residues incorporate ^{13}C at the C^{α} position with a yield of close to 30%, with a level on the order of 20% obtained for those residues that use the AKG precursor. Labeling is more efficient for the OA derived residues in comparison to those produced from AKG, as expected, because OA can be directly synthesized by carboxylation of PEP and molecules produced in this

Table 1 ^{13}C enrichment levels at C^{α} positions and at methyl positions using either [2-^{13}C]-Glc or [1-^{13}C]-Glc as the carbon source[a]

Residues	Precursor(s)	Enrichment	Position
Ala, Cys, Gly, Phe, Ser, Trp, Tyr, Val	Pyruvate, 3-phosphoglycerate, phosphoenolpyruvate	0.45 ± 0.04 (23)[c]	C^{α}
Asn, Asp, Ile, Met, Thr	Oxaloacetate	0.28 ± 0.02 (21)[c]	
Arg, Gln, Glu, Pro	α-ketoglutarate	0.17 ± 0.02 (17)	
Lys	Oxaloacetate or pyruvate	0.38 ± 0.03 (11)	
His	Ribose-5-phosphate	0.30 ± n.a. (1)	
Leu[b]	Acetyl-S-CoA	0.06 ± 0.01 (7)	
Ala, Ile$^{\gamma 2}$, Leu, Val	Pyruvate	0.44 ± 0.02 (41)	methyl
Ile$^{\delta 1}$, Thr	Oxaloacetate	0.13 ± 0.01 (13)[d]	
Met	N^5-methyl-THF	0.35 ± 0.01 (5)	

[a] C^{α} enrichment levels are based on data from ubiquitin and the FBP11 FF domain, while methyl enrichment levels are calculated from measurements recorded on ACBP and the FF domain. Residues are grouped based on which precursor they are derived from (see Figs. 1 and 2) and the results for all residues within a group and from both proteins measured to quantify a given enrichment level are averaged

[b] C^{α} of Leu is derived from the methyl group of acetyl-S-CoA as shown in Fig. 2. This position is not expected to be enriched if [2-^{13}C]-Glc is used as the carbon source according to the major biosynthetic pathways

[c] For Ile and Val (only) both $^{13}C^{\alpha}$–$^{12}C^{\beta}$ and $^{13}C^{\alpha}$–$^{13}C^{\beta}$ moieties are observed in relative proportions of 1.2:1

[d] For Ile$^{\delta 1}$ and Thr (only) 25% of ^{13}C labeled methyl groups are directly attached to a ^{13}C spin (i.e., 75% are isolated)

manner will have an enrichment level of close to 50% at position 2. In contrast, the AKG derived residues produced with $^{13}C^{\alpha}$ must rely on two steps of the TCA cycle that dilutes the ^{13}C label. The level of ^{13}C enrichment for Lys is close to 40% and is expected to be higher than for the residues that derive from OA (~30%) since C^{α} of Lys originates either from position 2 of OA or from position 2 of pyruvate that can be directly transferred without dilution. Finally, the value obtained for His must be considered very tentative since only 1 residue of this type was present in the 2 proteins examined and, as expected, essentially no incorporation could be detected for Leu (6%).

Figure 4b shows correlations from expanded methyl regions of the ^{1}H–^{13}C correlation map of the FBP11 FF domain produced using [1-^{13}C]-Glc as the carbon source with the multiplet structures highlighted. Correlations for all residues with the exception of Ile and Thr are singlets while those for Ile($C^{\delta 1}$) and Thr methyls are superpositions of doublets (with splittings on the order of 35 Hz) and singlets, indicating that a fraction of the ^{13}C-labeled methyl groups for these residues are directly coupled to ^{13}C spins. Notably, correlations from the Ile($C^{\gamma 2}$) methyl position are all singlets. These observations are consistent with expectations based on the metabolic pathways discussed above. Methyl groups derived from glycolysis intermediates such as pyruvate will be isolated since pyruvate is labeled at only a single position. By contrast, methyl groups produced from TCA cycle intermediates that can be multiply labeled (see Fig. 2) need not be isolated.

The level of incorporation of ^{13}C into methyl positions of the methyl containing amino acids is summarized in Table 1 (bottom three rows) with quantification achieved as described above for labeling at the C^{α} position. As expected, methyl groups derived from pyruvate are enriched at levels close to 50% (44%). Ile($C^{\delta 1}$) and Thr($C^{\gamma 2}$) are derived from OA that can be (but does not have to be) multiply labeled (Fig. 2) and hence lower yields of isolated ^{13}C labeled methyl groups are expected for these residues. As indicated above, the Met methyl derives from a methyl group carried by tetrahydrofolate that originates from the C^{β} position of Ser. It is interesting that although Ser would be expected to be labeled to ~45% at the C^{β} position, based on the results of the present analysis, the incorporation of ^{13}C methyl label into Met is somewhat lower, 35%. Finally, it is worth noting that the positions that become labeled with [1-^{13}C]-Glc are to a great extent the same as those when [3-^{13}C]-pyruvate is used as the carbon source. However, a noteworthy difference is that isolated C^{β} groups are produced for Ala with [1-^{13}C]-Glc, in contrast to previous observations for growth on [3-^{13}C]-pyruvate (Mulder et al. 2002).

In principle, the levels of enrichment quantified above for the OA and AKG based residues are expected to depend on growth conditions and bacterial strains. For example, particularly relevant is the rate of conversion of PEP into Asp (via OA; Fig. 1) relative to the rate of entry of OA into the TCA cycle. If the flux through the TCA cycle is reduced to zero the expected enrichment at the C^{α} position ([2-^{13}C]-Glc) for Asp and hence Asn, Ile, Lys, Met, Thr that follow from Asp would be expected to be 50%. Lower enrichments would be expected for these residues as the TCA flux increases due to scrambling of label. Similarly, those strains with an active glyoxylate shunt, leading to the conversion of isocitrate to malate without formation of AKG, would contain lower levels of $^{13}C^{\alpha}$ Glu and labeled Arg, Gln and Pro that derive from Glu since less labeled

precursor AKG would be produced. It has been reported that in JM109 cells the relative flux rates of PEP into OA versus entry of OA into the TCA cycle is three fold higher than for BL21 cells (Noronha et al. 2000) and it is thus expected that increased label would be observed for OA derived residues in proteins produced in JM109. We have investigated this qualitatively by producing ubiquitin in BL21 cells while the FF domain from FBP11 was generated in JM109 cell lines and subsequently comparing label incorporation. Surprisingly, however, the expected increase in enrichment level at C^{α} positions of residues produced from OA was not observed for the FF domain (JM109 cells). Indeed, in our experience the level of incorporation of label into both C^{α} and methyl positions is uniform from one protein to the next, with similar results obtained for proteins produced in the different laboratories that contributed to this work.

The labeling patterns generated using [1-^{13}C]-Glc and [2-^{13}C]-Glc are similar to those obtained using approaches described by LeMaster and Kushlan involving [1,3-$^{13}C_2$]-glycerol and [2-^{13}C]-glycerol, respectively, that produced alternating carbon enrichment (LeMaster and Kushlan 1996). Enrichment levels in excess of 90% at C^{α} were reported for all residues except the AKG group (~70%) and Leu (no enrichment) when [2-^{13}C]-glycerol and NaH$^{13}CO_3$ were used as carbon sources for expression of *E. coli* thioredoxin in a bacterial strain deficient in succinate and malate dehydrogenases. As expected these figures are higher than those presented here and considering that the cost of [2-^{13}C]-Glc and [2-^{13}C]-glycerol are approximately equal, the LeMaster approach is a very attractive option. It does suffer from a number of disadvantages, however. First, a modified *E. coli* strain must be employed that can be problematic for the expression of some proteins. Second, Ile and Val are produced with > 90% label at both $C^{\alpha}$and C^{β} positions, so that they cannot be probed by experiments that require isolated spin pairs. In contrast, significant populations of $^{13}C^{\alpha}$–$^{12}C^{\beta}$ relative $^{13}C^{\alpha}$–$^{13}C^{\beta}$ Ile and Val (in a 1.2:1 ratio) are obtained using [2-^{13}C]-Glc so that experiments that measure relaxation properties of isolated $^{13}C^{\alpha}$ spins can be performed so long as suitable purging pulse sequences are developed (to remove $^{13}C^{\alpha}$–$^{13}C^{\beta}$ pairs). LeMaster and Kushlan also reported that by using [1,3-$^{13}C_2$]-glycerol and NaH$^{12}CO_3$ the methyl groups of Ala, Ile($C^{\gamma 2}$), Leu and Val in *E. coli*. thioredoxin were enriched to more than 90% and Met to 80% (LeMaster and Kushlan 1996). In this case there is no need for modified *E. coli* strains but since the price of [1,3-$^{13}C_2$]-glycerol is almost four times that of [1-^{13}C]-Glc that is used here for the production of proteins with approximately 50% ^{13}C-methyl-labeling we feel that glucose is an excellent alternative.

The above discussion makes it clear that the singly ^{13}C-labeled glucoses, [2-^{13}C]-Glc and [1-^{13}C]-Glc, can be used to produce proteins with isolated ^{13}C labels at C^{α} or methyl positions, respectively. In the case of expression using [2-^{13}C]-Glc isolated $^{13}C^{\alpha}$ labels are generated for 17 of the 20 residue types, while an additional two residues (Ile and Val) contain either $^{13}C^{\alpha}$–$^{13}C^{\beta}$ or $^{13}C^{\alpha}$–$^{12}C^{\beta}$ label. In applications that require the quantification of relaxation of isolated spins, such as would be the case for CPMG-based relaxation dispersion analyses, for example, pulse schemes can be constructed to purge the undesired $^{13}C^{\alpha}$–$^{13}C^{\beta}$ spin pairs, as has been described previously (Mulder et al. 2002). Of the seven different methyl group probes, isolated methyl label is obtained at five positions using [1-^{13}C]-Glc (Thr and Ile($C^{\delta 1}$) are the two exceptions) that facilitates the study of dynamics at a wide range of hydrophobic sites in proteins.

As discussed very briefly above, there are a number of important spin relaxation applications that benefit significantly from the selective ^{13}C labeling that is introduced at C^{α} or methyl positions using the glucose precursors described here. One such example involves the measurement of $^{13}C^{\alpha}$ R_1 and $R_{1\rho}$ relaxation rates along with ^{1}H–^{13}C steady state NOE values that can be used to obtain insight into ps-ns time-scale motions involving the protein backbone that complement similar ^{15}N studies. Figure 5 shows R_1 (top row) and $R_{1\rho}$ (bottom) decay curves for a number of residues in ubiquitin that has been produced using [2-^{13}C]-Glc, including for S57 where $\varpi_{C\alpha} = 61.08$ ppm and $\varpi_{C\beta} = 62.53$ ppm. In the case of a $^{13}C^{\alpha}$–$^{13}C^{\beta}$ spin pair with these chemical shifts and for a 2 kHz spin lock field centered at 58.2 ppm and applied for a duration of up to 50 ms a maximum magnetization transfer from $^{13}C^{\alpha}$ to $^{13}C^{\beta}$ of 10% is predicted, giving rise to non-exponential decays of $^{13}C^{\alpha}$ magnetization in $R_{1\rho}$ type of experiments. By contrast, exponential decays are observed for all residues in ubiquitin. Finally, the absence of one-bond coupled neighbors simplifies the analysis of R_1 decay rates since cross-relaxation effects involving ^{13}C–^{13}C pairs that scale with molecular tumbling time are no longer an issue (Yamazaki et al. 1994).

One particularly powerful application of transverse spin-relaxation measurements involves the quantification of chemical exchange processes that provides unique information relating to the kinetics and thermodynamics of the exchange event(s) as well as insight into the structural features of potentially low populated 'invisible' states that participate in the exchange reaction (Grey et al. 2003; Korzhnev et al. 2004). These experiments are most readily performed on samples with isolated label, as homonuclear scalar coupling effects can complicate or even prevent accurate interpretation of the data (Ishima et al. 2004). For example, one important class of experiment measures ms

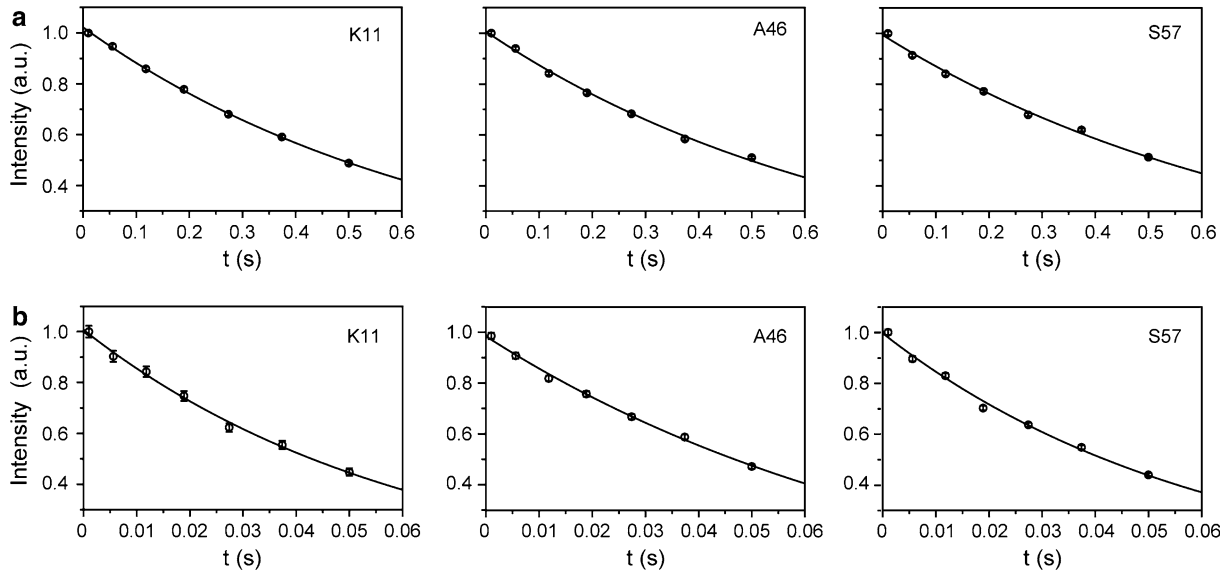

Fig. 5 R_1 and $R_{1\rho}$ decays for residues K11, A46 and S57 of U-^{15}N/[2-^{13}C]-Glc ubiquitin recorded at 800 MHz, 25°C. The lines represent the best fit to a decaying mono-exponential function. (**a**) The R_1 rates are 1.47 ± 0.03 s^{-1}, 1.41 ± 0.02 s^{-1} and 1.32 ± 0.02 s^{-1} respectively. (**b**) The $R_{1\rho}$ experiment was performed with a spin-lock field of 1790 Hz, with the carrier positioned at 58.2 ppm so that the effective spin-lock fields are tilted at angles of 78.1°, 57.3° and 108.4° with respect to the positive z-axis for K11, A46 and S57, respectively. The $R_{1\rho}$ rates are 16.3 ± 0.7 s^{-1}, 11.8 ± 0.3 s^{-1}, 16.5 ± 0.3 s^{-1}, respectively

time-scale exchange through the application of a train of 180° pulses that refocuses chemical shift evolution (in the absence of exchange) but not the effects of homonuclear scalar couplings. One bond aliphatic ^{13}C–^{13}C couplings are particularly deleterious because of their large size (35 Hz) that leads to significant signal modulations that depend in a complex manner on the number of refocusing pulses. Figure 6 shows $^{13}C^{\alpha}$ CPMG relaxation dispersion profiles recorded on an F61A/A90G Rd-apoctychrome b_{562} sample prepared using [2-^{13}C]-Glc. These data sets are recorded in a manner very similar to ^{15}N dispersion profiles (Tollinger et al. 2001), where effective relaxation rates are measured as a function of the number of refocusing pulses applied during a constant-time period of duration T. $R_{2,eff}$ is then defined according to the relation

$$R_{2,eff}(\nu_{CPMG}) = -1/T \ln(I(\nu_{CPMG})/I_o) \quad (1)$$

where $\nu_{CPMG} = 1/(2\delta)$, δ is the time between refocusing pulses and $I(\nu_{CPMG})$ and I_o are the intensities of correlations recorded in spectra obtained with and without the CPMG elements. Dispersion data sets were acquired at static magnetic field strengths of 500 (lower trace) and 800 MHz spectrometer fields and data for 35 residues for which $R_{2,eff}$(125 Hz) – $R_{2,eff}$(875 Hz) > 5 s^{-1} were fit simultaneously to a 2-site model of chemical exchange, $A \rightleftarrows^{k_A}_{k_B} B$. Values of $k_{ex} = k_A + k_B = 1230 \pm 35$ s^{-1} and $p_B = 2.4 \pm 0.04\%$ were obtained (45°C), that are in reasonable agreement with exchange parameters isolated from fits of ^{15}N dispersion curves measured on the same sample, $k_{ex} = 1270 \pm 20$ s^{-1} and $p_B = 1.9 \pm 0.02\%$. The exchange parameters are also similar to those from previously published ^{15}N data where it was shown that the exchange contributions derive from a folding/unfolding process (Choy et al. 2005). Notably, the ^{13}C chemical shifts of the minor state that have been extracted from fits of dispersion profiles agree well with those expected for an unfolded conformation (data not shown). It is important to emphasize that although the agreement with ^{15}N data is reasonable, the population of the minor state obtained from the $^{13}C^{\alpha}$ data is somewhat higher than that generated from fits of the ^{15}N profiles. We have noticed this for several other protein systems as well and work is in progress to understand the origin of this difference.

A selection of methyl relaxation dispersion profiles from the FBP11 FF domain prepared using [1-^{13}C]-Glc is shown in Fig. 7. An analysis of 15 dispersion profiles recorded at 500 and 800 MHz, 30°C, satisfying $R_{2,eff}$(67 Hz) – $R_{2,eff}$(1000 Hz) > 1.4 s^{-1} using a two-site exchange model produced values of $k_{ex} = 2420 \pm 50$ s^{-1} and $p_B = 2.2 \pm 0.06$ % that are in good agreement with $k_{ex} = 2290 \pm 25$ s^{-1} and $p_B = 2.3 \pm 0.06$ % measured on the same sample via ^{15}N dispersion methods.

An additional application that benefits from isolated ^{13}C labeling is one where sub-ms time-scale dynamics are probed using off-resonance $R_{1\rho}$ experiments. We have previously published an experiment that measures $R_{1\rho}$ rates of $^{13}CHD_2$ labeled methyl groups in U-^{13}C, fractionally ^{2}H labeled proteins (Brath et al. 2006). One problem that emerges with uniform labeling is Hartmann-Hahn transfer

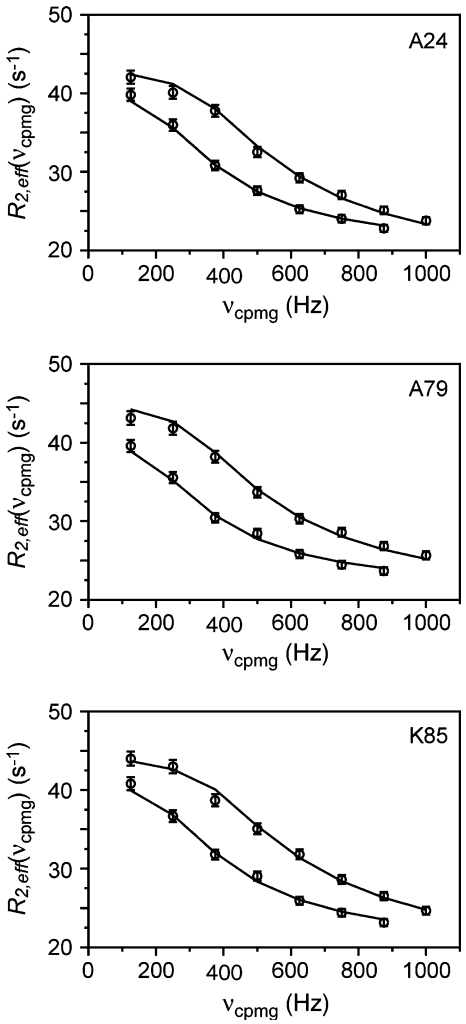

Fig. 6 $^{13}C^{\alpha}$ CPMG relaxation dispersion profiles for residues A24, A79 and K85 of U-^{15}N/[2-^{13}C]-Glc F61A/A90G Rd-apoctychrome b_{562}. Upper (lower) symbols denote data points recorded at 800 MHz (500 MHz) and the solid lines derive from a simultaneous fit of data from all residues with $R_{2,eff}$(125 Hz) - $R_{2,eff}$(875 Hz) > 5 s^{-1} to a global two state exchange process. The chemical shift differences between the two states for A24, A79 and K85 are 2.52 ± 0.09 ppm, 2.29 ± 0.09 ppm and 2.68 ± 0.10 ppm respectively

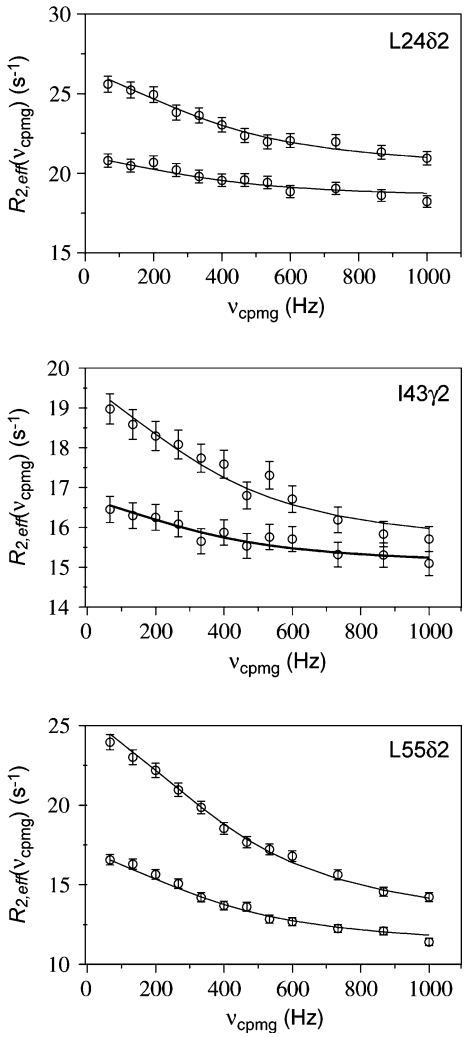

Fig. 7 ^{13}C methyl CPMG dispersion profiles for L24δ2, I43γ2 and L55δ2 of a U-^{15}N/[1-^{13}C]-Glc FBP11 FF domain. Upper (lower) traces are recorded at 800 MHz (500 MHz) and the solid lines derive from simultaneous fits of the data at the two fields to a global two state process. The chemical shift differences between the two states for L24δ2, I43γ2 and L55δ2 are 0.72 ± 0.02 ppm, 0.56 ± 0.02 ppm and 1.12 ± 0.02 ppm, respectively

between the methyl probe and its directly attached carbon that for certain residues (such as Leu) and for certain carrier offsets (for example, in between the spins in question) can be particularly troublesome. Of course, this problem is avoided for isolated spins so that robust measures of $R_{1\rho}$ rates and subsequently exchange parameters can be obtained. With these advantages in mind we have prepared a sample of ACBP with [1-^{13}C]-Glc and 98% D_2O (*E. coli* culture). Using this expression medium one might expect that the ^{13}C labeled pyruvate generated during glycolysis would be of the $^{13}CHD_2$ variety since two of the methyl protons originate from the solvent and thus methyl groups in the protein would appear as the $^{13}CHD_2$ isotopomer. In fact, for ACBP studied here all three of the ^{1}H-containing isotopomers, $^{13}CHD_2$, $^{13}CH_2D$ and $^{13}CH_3$ are observed in correlation spectra with relative populations of approximately 0.65, 0.3 and 0.05, respectively. The populations of the $^{13}CH_2D$ and $^{13}CH_3$ isotopomers are greater than what would be expected from the approximately 2% H_2O in the media, possibly due to isotope selection by the enzymatic steps where protons are added; nevertheless the $^{13}CHD_2$ isotopomer, as predicted, is dominant. The dominance of the $^{13}CHD_2$ isotopomer over $^{13}CH_3$ is advantageous because filtering to exclude the $^{13}CH_3$ moieties from the spectrum is inefficient due to ^{1}H–^{1}H cross-correlated relaxation in the $^{13}CH_3$ group (Ishima et al. 1999). Thus,

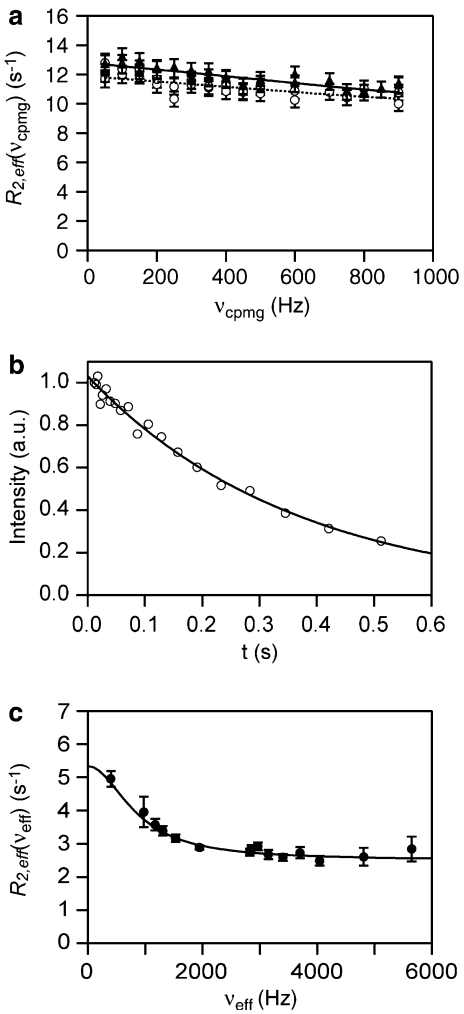

Fig. 8 ^{13}C CPMG and $R_{1\rho}$ relaxation dispersion profiles from one of the L15 C^{δ} methyl groups of ACBP (methyls are not stereospecifically assigned). The data from the two experiments were fitted together to a two-state exchange model. (**a**) ^{13}C CPMG relaxation dispersion data from a sample produced with [1-^{13}C]-Glc, H_2O. Filled (open) symbols indicate data recorded at 600 (500) MHz. (**b**) Representative $R_{1\rho}$ decay for L15 C^{δ} obtained with a nominal tilt-angle of 90° and a spin-lock field of 2825 Hz. The solid line is the best fit to a mono-exponential function that yields $R_{1\rho} = 2.77 \pm 0.10$ s^{-1}. (**c**) Effective relaxation rate as a function of effective spin-lock field, ν_{eff} for ACBP ([1-^{13}C]-Glc, D_2O). The solid and dashed in (**a**) and (**c**) are derived from a combined fit of the CPMG and $R_{1\rho}$ relaxation dispersion data sets

the residual intensity from the $^{13}CH_3$ isotopomer is minimized compared to that obtained on samples prepared with alternative carbon sources, such as [3-^{13}C]-pyruvate or [U-$^{13}C_6$]-Glc. Figure 8 illustrates combined fits of CPMG (a) and $R_{1\rho}$ (c) relaxation dispersion profiles for one of the methyl groups of Leu15 of ACBP, providing information on the folding-unfolding transition of this protein. From this data $k_{ex} = (5.0 \pm 0.7) \cdot 10^3$ s^{-1}, $|\Delta\varpi| = 2.5 \pm 0.7$ ppm and $p_U = 0.4 \pm 0.2\%$ are extracted; it is clear that CPMG data alone is not sufficient to adequately characterize dynamics on this time-scale.

In summary, we have presented a simple approach for the production of selectively ^{13}C-labeled proteins that is based on growth in either [1-^{13}C]-Glc or [2-^{13}C]-Glc media. The use of [1-^{13}C]-Glc produces proteins where 5 of the 7 methyl groups in methyl containing residues are enriched in ^{13}C without one-bond ^{13}C–^{13}C scalar couplings that would normally interfere with accurate spin-relaxation measurements. Protein production using [2-^{13}C]-Glc leads to enrichment of ^{13}C at C^{α} positions without incorporation of label at either C^{β} or CO sites for 17 residue types. A large number of 'isolated' backbone and methyl side-chain probes are thus available for the study of protein dynamics that complement nicely ^{15}N measures of motion. Although focus here has been on the generation of proteins with label at either C^{α} or methyl positions it is also the case that isolated ^{13}C sites are produced at other positions using the glucose precursors described here (Teilum et al. 2006) that will provide further probes of molecular dynamics.

Acknowledgments P.L., K.T. and D.F.H. are supported by fellowships from the Hellmuth Hertz foundation, EMBO and The Danish Agency for Science, Technology and Innovation (J.no. 272-05-0232), respectively. Useful discussions with Prof. Mike Rosen (University of Texas Southwestern Medical School) are acknowledged. This research was supported by grants from the Canadian Institutes of Health Research (L.E.K.) and the Swedish Research Council (M.A.). L.E.K. holds a Canada Research Chair in Biochemistry.

References

Brath U, Akke M, Yang DW, Kay LE, Mulder FAA (2006) Functional dynamics of human FKBP12 revealed by methyl C-13 rotating frame relaxation dispersion NMR spectroscopy. J Am Chem Soc 128:5718–5727

Choy WY, Zhou Z, Bai YW, Kay LE (2005) An N-15 NMR spin relaxation dispersion study of the folding of a pair of engineered mutants of apocytochrome b(562). J Am Chem Soc 127:5066–5072

Chu R, Takei J, Knowlton JR, Andrykovitch M, Pei WH, Kajava AV, Steinbach PJ, Ji XH, Bai YW (2002) Redesign of a four-helix bundle protein by phage display coupled with proteolysis and structural characterization by NMR and x-ray crystallography. J Mol Biol 323:253–262

Cordier F, Brutscher B, Marion D (1996) Measurement of C-13(alpha)-(CO)-C-13 cross-relaxation rates in N-15-(IC)-C-13-labeled proteins. J Biomol NMR 7:163–168

Delaglio F, Grzesiek S, Vuister GW, Zhu G, Pfeifer J, Bax A (1995) NMRPipe—a multidimensional spectral processing system based on unix pipes. J Biomol NMR 6:277–293

Di Stefano DL, Wand AJ (1987) Two-dimensional H-1-NMR study of human ubiquitin: a main chain directed assignment and structure analysis. Biochemistry 26:7272–7281

Fruh D, Tolman JR, Bodenhausen G, Zwahlen C (2001) Cross-correlated chemical shift modulation: A signature of slow internal motions in proteins. J Am Chem Soc 123:4810–4816

Geen H, Freeman R (1991) Band-selective radiofrequency pulses. J Magn Reson 93:93–141

Goddard TD and Kneller DG SPARKY 3, University of California, San Francisco

Grey MJ, Wang CY, Palmer AG, III (2003) Disulfide bond isomerization in basic pancreatic trypsin inhibitor: Multisite chemical exchange quantified by CPMG relaxation dispersion and chemical shift modeling. J Am Chem Soc 125:14324–14335

Ishima R, Baber J, Louis JM, Torchia DA (2004) Carbonyl carbon transverse relaxation dispersion measurements and ms-mu s timescale motion in a protein hydrogen bond network. J Biomol NMR 29:187–198

Ishima R, Louis JM, Torchia DA (1999) Transverse C-13 relaxation of CHD2 methyl isotopmers to detect slow conformational changes of protein side chains. J Am Chem Soc 121:11589–11590

Ishima R, Louis JM, Torchia DA (2001) Optimized labeling of (CHD2)-C-13 methyl isotopomers in perdeuterated proteins: Potential advantages for C-13 relaxation studies of methyl dynamics of larger proteins. J Biomol NMR 21:167–171

Jemth P, Day R, Gianni S, Khan F, Allen M, Daggett V, Fersht AR (2005) The structure of the major transition state for folding of an FF domain from experiment and simulation. J Mol Biol 350:363–378

Kay LE, Torchia DA, Bax A (1989) Backbone dynamics of proteins as studied by N-15 inverse detected heteronuclear NMR-spectroscopy - application to Staphylococcal nuclease. Biochemistry 28:8972–8979

Korzhnev DM, Salvatella X, Vendruscolo M, Di Nardo AA, Davidson AR, Dobson CM, Kay LE (2004) Low-populated folding intermediates of Fyn SH3 characterized by relaxation dispersion NMR. Nature 430:586–590

Le HB, Oldfield E (1994) Correlation between N-15 NMR chemical-shifts in proteins and secondary structure. J Biomol NMR 4:341–348

Lee AL, Urbauer JL, Wand AJ (1997) Improved labeling strategy for C-13 relaxation measurements of methyl groups in proteins. J Biomol NMR 9:437–440

LeMaster DM, Kushlan DM (1996) Dynamical mapping of *E. coli* thioredoxin via C-13 NMR relaxation analysis. J Am Chem Soc 118:9255–9264

Loria JP, Rance M, Palmer AG, III (1999) A relaxation-compensated Carr-Purcell-Meiboom-Gill sequence for characterizing chemical exchange by NMR spectroscopy. J Am Chem Soc 121:2331–2332

Lundström P, Vallurupalli P, Religa TL, Dahlquist FW, Kay LE (2007) A single-quantum methyl C-13-relaxation dispersion experiment with improved sensitivity. J Biomol NMR 38:79–88

Mandrup S, Hojrup P, Kristiansen K, Knudsen J (1991) Gene synthesis, expression in *Escherichia Coli*, purification and characterization of the recombinant bovine acyl-CoA-binding protein. Biochem J 276:817–823

Mittermaier A, Kay LE (2006) New tools provide new insights in NMR studies of protein dynamics. Science 312:224–228

Mulder FAA, Hon B, Mittermaier A, Dahlquist FW, Kay LE (2002) Slow internal dynamics in proteins: Application of NMR relaxation dispersion spectroscopy to methyl groups in a cavity mutant of T4 lysozyme. J Am Chem Soc 124:1443–1451

Mulder FAA, Mittermaier A, Hon B, Dahlquist FW, Kay LE (2001) Studying excited states of proteins by NMR spectroscopy. Nat Struct Biol 8:932–935

Nicholson LK, Kay LE, Baldisseri DM, Arango J, Young PE, Bax A, Torchia DA (1992) Dynamics of methyl-groups in proteins as studied by proton-detected C-13 NMR-spectroscopy - application to the leucine residues of Staphylococcal nuclease. Biochemistry 31:5253–5263

Noronha SB, Yeh HJC, Spande TF, Shiloach J (2000) Investigation of the TCA cycle and the glyoxylate shunt in Escherichia coli BL21 and JM109 using C-13-NMR/MS. Biotechnol Bioeng 68:316–327

Ottiger M, Bax A (1997) An empirical correlation between amide deuterium isotope effects on C-13(alpha) chemical shifts and protein backbone conformation. J Am Chem Soc 119:8070–8075

Palmer AG, III (2004) NMR characterization of the dynamics of biomacromolecules. Chem Rev 104:3623–3640

Palmer AG, III, Kroenke CD, Loria JP (2001) Nuclear magnetic resonance methods for quantifying microsecond-to-millisecond motions in biological macromolecules. Method Enzymol 339:204–238

Peng JW, Wagner G (1994) Investigation of Protein Motions Via Relaxation Measurements. Method Enzymol 239:563–596

Press WH, Flannery BP, Teukolsky SA, Vetterling WT (1988) Numerical recipes in C. University Press, Cambridge

Skrynnikov NR, Mulder FAA, Hon B, Dahlquist FW, Kay LE (2001) Probing slow time scale dynamics at methyl-containing side chains in proteins by relaxation dispersion NMR measurements: Application to methionine residues in a cavity mutant of T4 lysozyme. J Am Chem Soc 123:4556–4566

Spera S, Bax A (1991) Empirical correlation between protein backbone conformation and C-alpha and C-beta C-13 nuclear magnetic resonance chemical shifts. J Am Chem Soc 113:5490–5492

Teilum K, Brath U, Lundström P, Akke M (2006) Biosynthetic C-13 labeling of aromatic side chains in proteins for NMR relaxation measurements. J Am Chem Soc 128:2506–2507

Tollinger M, Skrynnikov NR, Mulder FAA, Forman-Kay JD, Kay LE (2001) Slow dynamics in folded and unfolded states of an SH3 domain. J Am Chem Soc 123:11341–11352

Torchia DA, Ishima R (2003) Molecular structure and dynamics of proteins in solution: Insights derived from high-resolution NMR approaches. Pure App Chem 75:1371–1381

Voet D, Voet JG (1995) Biochemistry. John Wiley & Sons, Inc., Hoboken

Wand AJ, Bieber RJ, Urbauer JL, McEvoy RP, Gan ZH (1995) Carbon relaxation in randomly fractionally C-13-enriched proteins. J Magn Reson Ser B 108:173–175

Wang TZ, Cai S, Zuiderweg ERP (2003) Temperature dependence of anisotropic protein backbone dynamics. J Am Chem Soc 125:8639–8643

Wishart DS, Sykes BD (1994) The C-13 chemical-shift index–a simple method for the identification of protein secondary structure using C-13 chemical-shift data. J Biomol NMR 4:171–180

Xu XP, Case DA (2002) Probing multiple effects on N-15, C-13 alpha, C-13 beta, and C-13 ' chemical shifts in peptides using density functional theory. Biopolymers 65:408–423

Yamazaki T, Muhandiram R, Kay LE (1994) NMR experiments for the measurement of carbon relaxation properties in highly enriched, uniformly C-13, N-15-labeled proteins–Application to C-13(alpha) carbons. J Am Chem Soc 116:8266–8278

Zeng L, Fischer MWF, Zuiderweg ERP (1996) Study of protein dynamics in solution by measurement of C-13(alpha)-(CO)-C-13 NOE and (CO)-C-13 longitudinal relaxation. J Biomol NMR 7:157–162